Importance of geometrical corrections to fusion barrier calculations for deformed nuclei

I. I. Gontchar,* M. Dasgupta, D. J. Hinde, R. D. Butt, and A. Mukherjee
Department of Nuclear Physics, Research School of Physical Sciences and Engineering, Australian National University, Canberra, Australian Capital Territory 0200, Australia
(Received 27 November 2001; published 19 February 2002)

In conventional calculations of fusion cross sections and barrier distributions, the nuclear potential is determined along the line joining the centers of the two nuclei. For deformed nuclei of finite size, this does not correspond to the minimum distance between the nuclear surfaces. Calculations are made using the minimum distance as the argument of the internucleus nuclear potential. The surface curvature correction to this potential is also included. These geometrical effects significantly change the near-barrier fusion cross sections and the shape of the barrier distribution.

DOI: 10.1103/PhysRevC.65.034610 PACS number(s): 25.70.Jj

I. INTRODUCTION

More than 20 years ago it was conclusively shown [1] that fusing nuclei ''remember'' their individual structures (in particular, quadrupole deformations) when fusion is decided. However, the precision of the measured fusion cross sections, σ, was not high enough to show sensitivity to the magnitude or sign of the static deformations of the reacting nuclei. In the early 1990s a method was proposed [2], that allows the measured σ to be converted into an experimental barrier distribution D by double differentiation with respect to the energy in the center-of-mass frame, E:

$$D(E)=\frac{d^2(E\sigma)}{dE^2}. \tag{1}$$

This is proportional to the probability of encountering a fusion barrier of height E. The practical application of this formula required improved the precision of cross-section measurement, with an uncertainty of $\sim 1\%$. Soon such measurements were made [3], and showed that the fusion cross sections and $D(E)$ in the near-barrier region are extremely sensitive both to static nuclear deformation [3] and to vibrational excitations of the colliding nuclei [4].

In order to interpret cross sections and barrier distributions, the simplified coupled channels code CCDEF [5] and its development CCMOD [6] were used extensively [7]. One of the basic ingredients of these codes is a semiclassical treatment of deformation through an angle-dependent potential. The nuclear part of this potential is of Woods-Saxon (WS) form

$$V_{WS}=\frac{V_0}{1+\exp\{[r-R_P(\theta_p)-R_T(\theta_t)]/a\}}, \tag{2}$$

where V_0 and a are the depth and the diffuseness parameters, and $\theta_p(\theta_t)$ is the angle between the symmetry axis of the projectile (target) nucleus and the beam direction.

A radius parameter r_0 may be used to define the radii of the projectile and target nuclei:

$$R_P(\theta_p)=r_0A_P^{1/3}f(\theta_p), \quad R_T(\theta_t)=r_0A_T^{1/3}f(\theta_t). \tag{3}$$

For simplicity, we will consider only the case where the projectile is spherical [i.e., $f(\theta_p)=1$], and the target nucleus is deformed with $f(\theta_t)$ given by

$$f(\theta_t)=\lambda^{-1}[1+\beta_2Y_{20}(\theta_t)+\beta_4Y_{40}(\theta_t)]. \tag{4}$$

Here λ guarantees volume conservation [8].

The numerator of the argument of the exponent in Eq. (2), for spherical reacting nuclei, looks like a surface-to-surface distance. This interpretation ignores the fact that the r_0 parameter entering Eq. (3) and the corresponding parameter for the nuclear density distribution are not necessarily equal. Moreover, in more realistic descriptions of nucleus-nucleus collisions, there are three different radius parameters: the first appears in the parametrization of the internucleus potential, the second defines the matter density distribution, and the third defines the charge distribution. In order to make our schematic consideration simple, we neglect this difference, interpreting $\Delta r=r-R_{P0}-R_{T0}$ as the surface-to-surface distance for spherical reactants ($R_{P0}=r_0A_P^{1/3}$, $R_{T0}=r_0A_T^{1/3}$).

For deformed nuclei, however, such an interpretation disregards two points. First, $\Delta r=r-R_{P0}-R_T(\theta_t)$ is not the minimum surface-to-surface distance (except for $\theta_t=0,\pi/2$). This is illustrated in Fig. 1, where the geometry and relevant variables for this case are shown. Second, the nuclear attraction between two nuclei depends upon the curvatures of their surfaces. Thus the surface curvature correction to the sphere-to-sphere nuclear potential can influence the height of fusion barrier. Following Refs. [9,10] we refer to the internucleus potential with Δr as the argument as for the ''center-line'' potential. If the minimum distance between the nuclear surfaces is used as the argument, this is referred to as the ''surface-to-surface'' potential.

Many works were devoted to closely related topics. The effect of the shortest surface-to-surface distance on the values of deformation parameters extracted from nuclear and Coulomb measurements was first discussed in Ref. [11]. The proximity theorem [12] states that the internuclear potential

*Permanent Address: Omsk State Railway University, pr. Marska 35, Omsk, RU-644046, Russia.

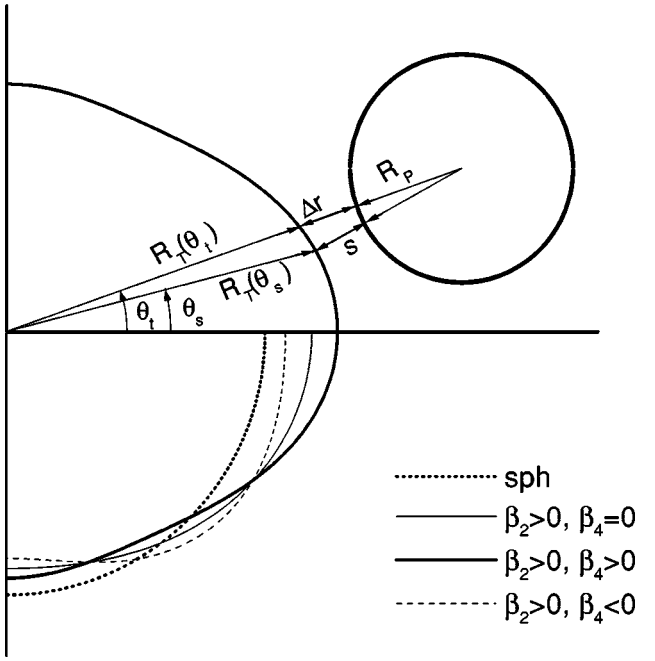

FIG. 1. Geometry of the interaction between spherical and deformed nuclei. Δr and s are the distances between the nuclear surfaces along the center line and along the perpendicular to both surfaces, respectively.

can be presented as a product of a function depending upon the shortest surface-to-surface distance, s, and a factor including the relevant geometry such as nuclear surface curvatures and the mutual orientation of the symmetry axes of the deformed reactants. In Refs. [10,13], the limits of applicability of the proximity theorem and its relation to the double folding potential were investigated. It was found that the proximity theorem provides an accurate description of the nuclear interaction between two nuclei when only one of the reactants is deformed [13]. In Refs. [9,10], it was found that the difference between the proximity and center-line potentials is particularly important in the presence of hexadecapole deformations.

The effect of the use of s instead of Δr as the argument of the nuclear potential for inelastic heavy-ion collisions was investigated in Refs. [10,14], and turned out to be substantial. However, to our knowledge it was never studied in calculations of heavy-ion fusion cross sections and barrier distributions. For example, in the calculations of Refs. [15,16] only a tip-to-tip geometry was considered, where $s=\Delta r$. In Ref. [17], in order to calculate the fusion cross sections, the exact single-folding potential for the nuclear interaction between nuclei possessing quadrupole deformation was used. However, in this work the center-line nucleon-nucleus WS potential, which ignores the difference between s and Δr, was used.

The purpose of this study is to show to what extent the calculated near-barrier fusion cross sections and the corresponding barrier distributions are sensitive to the use of the minimum distance s instead of Δr, and to the surface curvature correction to the nuclear potential. In Sec. II the nuclear and Coulomb potentials and their parameters are specified. In Sec. III the effect of using the surface-to-surface potential instead of the center-line potential is investigated for fusion barriers. Results of calculations of the fusion barriers, accounting for the surface curvature correction to the nuclear potential, are presented in Sec. IV. In Sec. V the fusion cross sections and barrier distributions are calculated and compared with experimental data. Conclusions are drawn in Sec. VI.

II. INPUT OF THE CALCULATIONS

For the Coulomb part of the nucleus-nucleus potential, we use the multipole expansion

$$V_C(r,\theta_t)=V_{sph}\{1+(R_{T0}/r)^2Y_{20}(\theta_t)[0.600\beta_2+0.216\beta_2^2 + 0.197\beta_4^2+0.579\beta_2\beta_4]/\lambda^5+(R_{T0}/r)^4Y_{40}(\theta_t) \times[0.242\beta_2^2+0.518\beta_4]/\lambda^7\}. \quad (5)$$

Here higher-order terms in quadrupole (β_2) and hexadecapole (β_4) deformations have been neglected.

For the center-line nuclear potential we use the single-folding potential of Refs. [16,18,19], which is obtained by folding the density of the projectile with the nucleon-nucleus (target) potential and vice versa. Both density and nucleon-nucleus potential have spherically symmetric WS shapes. For the density and the nucleon-nucleus potential we use the values of the parameters from Refs. [16,19]. According to Refs. [16,18] the resulting nucleus-nucleus potential is approximated as follows:

$$V_{FP}=\sum_{i=0}^{4} C_i(\Delta r)^i \ln[1+\exp(-\Delta r/a)]. \quad (6)$$

The meaning of r_0 and a for the V_{FP} is substantially different from that of the WS potential, since after r_0 and a are fixed, the coefficients C_i are found from the fit of Eq. (6) to the calculated folding potential. The standard values of the parameters of V_{FP} are $r_0=1.30$ fm and $a=0.61$ fm [16,19]. However, in determining C_i, we use $r_0=1.2$ fm to be consistent with the calculation of the values of the deformation parameters β_2 and β_4 (see below). The small change of r_0 from the standard value changes the calculated cross sections and barrier distributions only slightly. Since measurements of Refs. [1,3,7,20] were performed for ^{16}O-induced reactions, we concentrate on the $^{16}O+^{154}Sm$ reaction in what follows. The values of the deformation parameters of ^{154}Sm were taken to be $\beta_2=0.306$ [21] and $\beta_4=0.13$ [22]. Note that these values are close to those theoretically predicted in Ref. [23]: $\beta_2=0.270$ and $\beta_4=0.113$.

III. EFFECT OF THE MINIMUM DISTANCE BETWEEN NUCLEAR SURFACES

In this section we calculate the minimum distance between the surfaces s and the center-line and surface-to-surface barriers $B_{\Delta r}$ and B_s, as well as the corresponding barrier radii $r_{\Delta r}$ and r_s ignoring the surface curvature correction to the nuclear potential. In order to make calculations

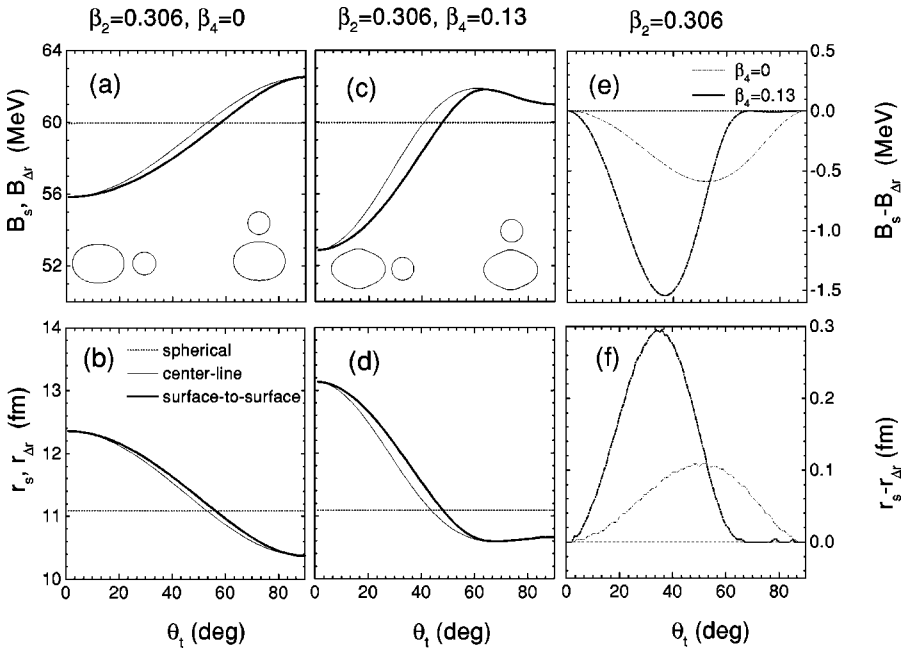

FIG. 2. Calculated $L=0$ fusion barriers for the center-line and surface-to-surface potentials for the $^{16}O+^{154}Sm$ reaction with quadrupole and hexadecapole deformations. As a function of polar angle θ_t, we show (a) and (c) the fusion barrier heights calculated with the surface-to-surface potential B_s (thick solid lines) and with the center-line potential $B_{\Delta r}$ (thin solid lines); (b) and (d) the barrier radii, r_s and $r_{\Delta r}$ [all the notations as in panels (a) and (c)]; (e) the differences between the barrier heights, $B_s-B_{\Delta r}$, calculated with $\beta_2=0.306$ and $\beta_4=0$ (thin line) and $\beta_2=0.306$ and $\beta_4=0.13$ (thick line); and (f) the differences between the barrier radii, $r_s-r_{\Delta r}$ [notations as in panel (e)]. The dotted lines in panels (a)—(d) correspond to the spherical target.

with the surface-to-surface potential we use s instead of Δr in Eq. (6). From the geometry shown in Fig. 1, one sees that the minimum distance can be found numerically from the following equations:

$$(s+R_{P0})^2=r^2+R_T^2(\theta_s)-2rR_T(\theta_s)\cos(\theta_s-\theta_t),$$
$$\frac{d(s+R_{P0})^2}{d\theta_s}=0. \tag{7}$$

In Fig. 2 we present results of the calculations for zero orbital angular momentum ($L\hbar$). All calculated quantities are plotted here versus polar angle θ_t. First we examine the effect of the surface-to-surface potential in the presence of only quadrupole deformation ($\beta_2=0.306$, $\beta_4=0$). Figure 2(a) shows that B_s is lower than $B_{\Delta r}$, as expected. For the barrier radii this is opposite, as shown in Fig. 2(b). Only at $\theta_t=0$ and $\pi/2$ are the results the same, since here Δr equals s.

Let us now consider the effect of hexadecapole deformation on the fusion barriers. The results, presented in Figs. 2(c) and 2(d), were obtained for $\beta_2=0.306$ and $\beta_4=0.13$. Qualitatively the effect of accounting for the minimum distance between the surfaces in this case is similar to the previous case. However quantitatively there are some differences. First, in Fig. 2(c) one sees that B_s and $B_{\Delta r}$ become indistinguishable over a rather wide equatorial range of θ_t. The same happens to r_s and $r_{\Delta r}$ in Fig. 2(d). This is because of the ''bulge''on the nuclear surface around the equator due to the positive hexadecapole deformation [see Fig. 1, and the inset in Fig. 2(c)]. Second, the range of variation of the barrier height [compare Figs. 2(a) and 2(c)] and radius [compare Figs. 2(b) and 2(d)] becomes significantly larger due to the sharper tip of the target nucleus in the presence of hexadecapole deformation [compare insets in Figs. 2(a) and 2(c)].

The differences in barrier heights, $B_s-B_{\Delta r}$, for the two cases, $\beta_2=0.306$ and $\beta_4=0.0$ (thin line), and $\beta_2=0.306$ and $\beta_4=0.13$ (thick line), is presented in Fig. 2(e). The maximum absolute value of this difference for $\beta_4=0.0$ is 0.6 MeV (at $\theta_t=54°$), which is $\sim$10% of the total range of the barrier heights variation due to deformation. The hexadecapole deformation increases the maximum difference $B_{\Delta r}-B_s$ up to 1.5 MeV, and shifts its position to $\theta_t=37°$. Finally, in Fig. 2(f) we present the corresponding difference of the barrier radii. Here again a strong enhancement of the effect of the use of surface-to-surface potential in the presence of hexadecapole deformation is observed.

The influence of the change of projectile was checked by performing calculations for ^{28}Si and ^{58}Ni. It turned out that the variation of the fractional change of the fusion barrier heights, $(B_s-B_{\Delta r})/B_{\Delta r}$, remains within $\sim$0.2% in the whole range of the polar angle (from 0° up to 90°) when switching from one projectile to another. This is also true when a Woods-Saxon internucleus potential is used.

To complete our consideration of the effect of changing from the center-line potential to the surface-to-surface potential we made calculations of fusion barriers and barrier radii for higher values of orbital angular momentum, for $L=30$ and 50. The results are plotted in Fig. 3, along with those for $L=0$, versus the polar angle θ_t. Calculations are again performed with $\beta_2=0.306$ and $\beta_4=0.13$. The higher the value

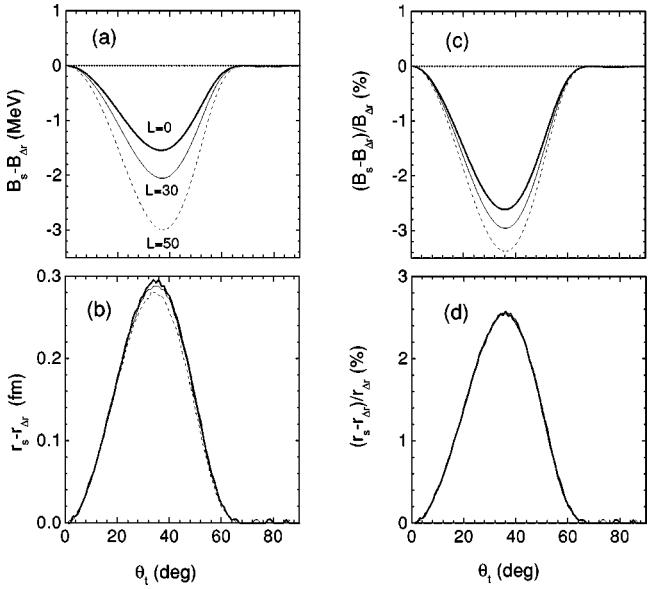

FIG. 3. The effect of using the surface-to-surface potential on the L-dependent fusion barriers. Shown for three values of orbital angular momentum [$L=0$ (thick solid lines), $L=30$ (thin solid lines), and $L=50$ (dashed lines)] are (a) the difference between the fusion barrier heights calculated with the surface-to-surface potential and with the center-line potential, $B_s - B_{\Delta r}$; (b) as in panel (a), but for the barrier radii, $r_s - r_{\Delta r}$; (c) fractional change of the fusion barrier heights, $(B_s - B_{\Delta r})/B_{\Delta r}$; and (d) same as in panel (c), but for the barrier radii. These calculations are performed for the ^{16}O $+^{154}$Sm reaction with $\beta_2 = 0.306$ and $\beta_4 = 0.13$. The dotted lines correspond to a spherical target.

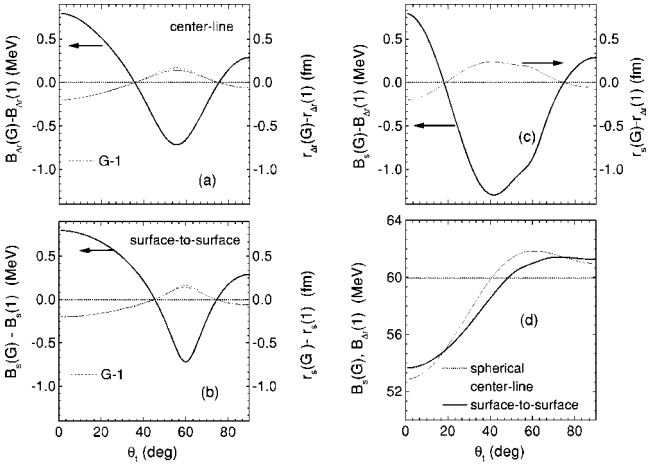

FIG. 4. Effect of accounting for the surface curvature correction for $L=0$ fusion barriers ($\beta_2 = 0.306, \beta_4 = 0.13$). As a function of polar angle θ_t we show (a) the difference between the center-line barrier calculated with and without curvature correction, $B_{\Delta r}(G) - B_{\Delta r}(1)$ (thick solid line), and the same difference for the barrier radii, $r_{\Delta r}(G) - r_{\Delta r}(1)$ (thin solid line), as well as $G-1$ (dashed line); (b) same as in panel (a) but for the surface-to-surface potential; (c) the difference between the surface-to-surface barrier calculated with the curvature correction and the center-line barrier without this correction, $B_s(G) - B_{\Delta r}(1)$, (thick solid line), and the same difference for the barrier radii, $r_s(G) - r_{\Delta r}(1)$, (thin solid line); and (d) fusion barrier calculated with the surface-to-surface potential including the curvature correction, $B_s(G)$, (thick solid line), with the center-line potential without the curvature correction, $B_{\Delta r}(1)$, (thin solid line), and for a spherical target (dotted line).

of L, the larger the absolute value of the difference $B_s - B_{\Delta r}$ [Fig. 3(a)]. There are two reasons for this. First, for higher partial waves the absolute value of the fusion barrier height increases due to the repulsive centrifugal potential. Second, due to this repulsion the reactants must come closer to each other in order to reach the fusion barrier; therefore, the effect of using the shortest surface-to-surface distance instead of Δr is enhanced. In the limiting case, one obtains $s=0$ when Δr is still positive. In order to separate the size of the second effect, in Fig. 3(c) we plot the fractional change of the heights of the surface-to-surface and center-line barriers. One sees that the effect of the use of surface-to-surface potential is enhanced for $L=50$ by up to $\sim 30\%$ in comparison with $L=0$. The L dependence of the difference of the barrier radii, $r_s - r_{\Delta r}$, is presented in Fig. 3(b), and is much weaker than the L dependence of $B_s - B_{\Delta r}$. The fractional difference $[r_s - r_{\Delta r}]/r_{\Delta r}$, shown in Fig. 3(d), is independent of L for all the values of the polar angle.

IV. SURFACE CURVATURE CORRECTION TO NUCLEAR POTENTIAL

According to the proximity theorem [12] the strength of the attraction between two nuclear surfaces is defined by the shortest distance between them, and the curvatures of the surfaces. However, the coefficients C_i in Eq. (6) are calculated for spherical targets and projectile nuclei. Therefore, in the case of statically deformed target nuclei the nuclear potential should be corrected for its angle-dependent surface curvature. This correction enters the calculations as a deformation- and angle-dependent factor G applied to the potential of Eq. (6) (see Refs. [15,16]),

$$G = \frac{(R_{P0} + R_{T0})}{\sqrt{[(1/R_{P0} + \kappa_1)(1/R_{P0} + \kappa_2)]}R_{T0}R_{P0}}, \qquad (8)$$

where $G=1$ for a spherical target nucleus. The principal curvatures κ_1 and κ_2 with respect to spherical coordinate angles θ and ϕ have been calculated according to Ref. [24].

The role of this curvature correction for zero orbital angular momentum and $\beta_2 = 0.306$ and $\beta_4 = 0.13$ is illustrated in Fig. 4. In this figure the quantities calculated, including the curvature correction, have "G" as the argument, whits those without this correction have the argument "1." First we made calculations with the center-line potential. Presented in Fig. 4(a) as a function of polar angle θ_t are the differences between the barrier heights $[B_{\Delta r}(G) - B_{\Delta r}(1)$ (thick solid line)] and the barrier radii $[r_{\Delta r}(G) - r_{\Delta r}(1)$ (thin solid line)] calculated with and without the curvature correction. The values of $G-1$ are shown by the dashed line. The curvature correction G is smaller than 1 (i.e., the nuclear attraction is weaker than between two spherical nuclei) around the equator and the tip of the target. This increases the height of the fusion barrier and decreases its radius. In the region $35° < \theta_t < 75°$ the barrier height is reduced and the barrier radius is increased because $G > 1$. The similarity in

the values of the dimensionless quantity $G-1$, and the barrier radii difference $r_{\Delta r}(G)-r_{\Delta r}(1)$ is coincidental.

A qualitatively similar behavior is found when using the surface-to-surface potential as presented in Fig. 4(b). Note that in this case the curvature correction is calculated at θ_s, not at θ_t.

The net effect of the surface-to-surface potential and curvature correction is shown in Fig. 4(c). Here the difference between the barrier heights calculated with the surface-to-surface potential accounting for the curvature correction, $B_s(G)$, and the barrier heights calculated according to the center-line potential without the curvature correction, $B_{\Delta r}(1)$, is shown by the thick solid line. The difference between the corresponding barrier radii, $r_s(G)-r_{\Delta r}(1)$, is shown by the thin solid line. Qualitatively the effect of the surface-to-surface potential and curvature correction together is similar to the effect of the curvature correction alone in Figs. 4(a) and 4(b). However, the range of the angles at which the barrier heights are reduced becomes wider. At these intermediate angles both effects work in the same direction, resulting in the maximum decrease of the fusion barrier heights by about 20% of the total range of the barrier variation due to deformation. The change of the absolute values of the barriers with polar angle θ_t is illustrated in Fig. 4(d). Let us recall that the minimum surface-to-surface distance effect disappears at the tip and equator (see Fig. 2) whereas the absolute value of $G-1$ reaches its local maxima at those points. Therefore, for θ_t near zero and 90°, $B_s(G)$ behaves essentially like $B_{\Delta r}(G)$.

Figure 5 illustrates the influence of angular momentum on the effects under discussion. These calculations have been made for values of $\theta_t=2°$, 45° and 88°, again for $\beta_2=0.306$ and $\beta_4=0.13$. In Fig. 5(a) the barriers calculated with the surface-to-surface potential, including curvature correction, are shown versus L. For comparison the L dependence of the barrier obtained for a spherical target is also shown by the dotted line. In Fig. 5(b) we present the difference $B_s(G)-B_{\Delta r}(1)$. As expected (see Fig. 4), the effect of the minimum surface-to-surface distance dominates at the intermediate angles ($\theta_t=45°$), whereas the curvature correction makes $B_s(G)$ larger than $B_{\Delta r}(1)$ near the tip and equator (the curves for $\theta_t=2°$ and 88°). For all values of the polar angle, the absolute value of the difference $B_s(G)-B_{\Delta r}(1)$ increases with L.

This behavior can be understood qualitatively from the approximate relation

$$B_s(G,L)-B_{\Delta r}(1,L)\approx B_s(G,0)-B_{\Delta r}(1,0)+bL(L+1)\times\left[\frac{1}{r_s^2(G,L)}-\frac{1}{r_{\Delta r}^2(1,L)}\right]. \quad (9)$$

Here $b=\hbar^2/2\mu$, μ is the reduced mass of the reactants. For the intermediate angles ($\theta_t=45°$), where the minimum surface-to-surface distance effect is enhanced by the curvature correction [$G>1$, see Fig. 4(c)] $B_s(G,0)<B_{\Delta r}(1,0)$, and $r_s(G,L)>r_{\Delta r}(1,L)$. This makes the difference of Eq. (9) negative, and its absolute value increases with L. Near the tip ($\theta_t=2°$) the minimum surface-to-surface distance effect is practically absent [see Fig. 2(c)], whereas the curvature correction G is smaller than 1 [see, e.g., Fig. 4(a)], which reduces nuclear attraction. Thus $B_s(G,0)>B_{\Delta r}(1,0)$ and $r_s(G,L)<r_{\Delta r}(1,L)$. Consequently, the difference of Eq. (9) is positive and increases with L. For the equatorial angles the situation is the same as for the tip.

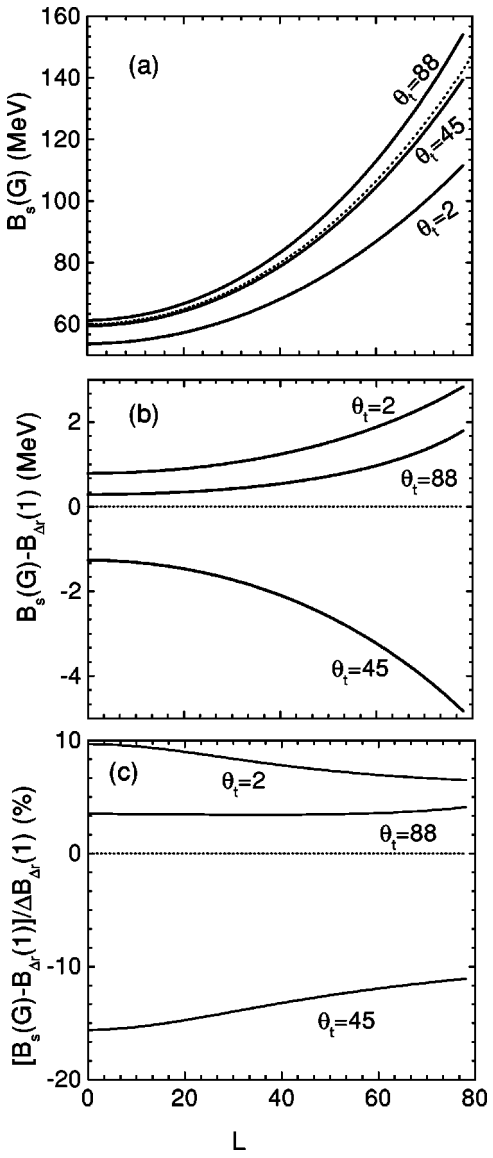

FIG. 5. The net effect of accounting for both the shortest surface-to-surface distance and the curvature correction on the heights of the L-dependent fusion barriers ($\beta_2=0.306$, $\beta_4=0.13$). Shown for three values of the polar angle θ_t, as a function of orbital angular momentum, are (a) the fusion barrier heights calculated with the surface-to-surface potential including the curvature correction, $B_s(G)$, (thick solid lines) and the barrier calculated for a spherical target (dotted line); (b) the difference between the heights of the barriers calculated with the surface-to-surface potential including the curvature correction and with the center-line barrier without this correction, $B_s(G)-B_{\Delta r}(1)$; and (c) the percentage of this barrier height difference with respect to the total range of the barrier height variation due to deformation as defined by Eq. (10).

Finally, it is very convenient to analyze the influence of L on the minimum distance and curvature effects by comparing

the difference $B_s(G)-B_{\Delta r}(1)$ with the total range of the barrier heights variation due to deformation, e.g., $\Delta B_{\Delta r}(1) = B_{\Delta r}(1,90°)-B_{\Delta r}(1,0°)$. The corresponding percentage,

$$\delta = \frac{B_s(G)-B_{\Delta r}(1)}{B_{\Delta r}(1,90°)-B_{\Delta r}(1,0°)}, \tag{10}$$

is shown in Fig. 5(c). It is interesting to see that the absolute values of δ either decrease slightly (at $\theta_t = 2°$ and 45°) or stay unchanged (at $\theta_t = 88°$). Qualitatively, the minimum distance and curvature effects do not change with L. Thus; one can expect that for low incident energies the fusion cross sections calculated with $B_s(G)$ will be lower than those calculated with $B_{\Delta r}(1)$, with the situation reversing as the collision energy is increased.

V. FUSION CROSS SECTIONS AND BARRIER DISTRIBUTIONS

The ultimate goal of our study is to see the effect of using the minimum surface-to-surface distance and curvature correction on the fusion cross sections and barrier distribution. Therefore, we now discuss calculations of these quantities and finally make a comparison with experimental data.

The transmission coefficients $T_L(\theta_t)$ have been calculated by means of the parabolic barrier approximation for each value of θ_t in the interval 0° to 90° with a step of 1°. Then the fusion cross sections have been found according to the formulas [7,20]

$$\sigma(L,\theta_t) = \left(\frac{\pi\hbar^2}{2\mu E}\right)\left(\frac{2L+1}{1+\exp\{2\pi[B(L,\theta_t)-E]/\hbar\omega(L,\theta_t)\}}\right), \tag{11}$$

$$\sigma = \sum_L \sum_0^{\pi/2} \sigma(L,\theta_t)\sin(\theta_t). \tag{12}$$

We found that the use of θ_t steps of 0.5° and 0.25° changes the cross sections and barrier distributions by less then 0.5%.

Quantum mechanically, one should consider the coupling of the relative motion of the reactants to the rotational motion of the deformed target. The classical approach, followed here, is an approximation which gives the result close to the full quantum mechanical calculation for well deformed nuclei (see e.g. Refs. [7,25]).

The calculated fusion cross sections and barrier distributions are shown in Fig. 6 versus the energy in the center of mass frame. Since statically deformed nuclei possess both positive and negative hexadecapole deformations, we made calculations for $\beta_4 = +0.13$ (left panels) and -0.13 (right panels), while keeping $\beta_2 = 0.306$ the same, in order to see the effect of the sign of the hexadecapole deformation. Three types of calculations of σ and D have been made. Two are without curvature correction, for the center-line potential [$\sigma_{\Delta r}(1)$ and $D_{\Delta r}(1)$, (dashed lines)], and for the surface-to-surface potential [$\sigma_s(1)$ and $D_s(1)$, (thin solid lines)]. The last is for the surface-to-surface potential including the curvature correction [$\sigma_s(G)$ and $D_s(G)$, (thick solid lines)].

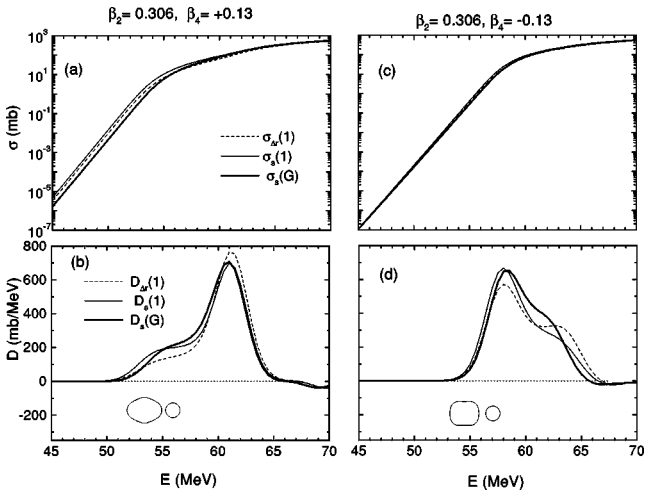

FIG. 6. Influence of the sign of the hexadecapole deformation on the fusion cross sections and barrier distributions. The calculated fusion cross sections σ [panels (a) and (c)] and the barrier distribution D [see Eq. (1)] [panels (b) and (d)] vs the energy in the center-of-mass frame E. Calculations an performed with $\beta_2 = 0.306$, and with $\beta_4 = +0.13$ (left panels) and $\beta_4 = -0.13$ (right panels). Dashed lines denote calculations without curvature correction with the center-line potential; thin solid lines are for calculations without the curvature correction with surface-to-surface potential; thick solid lines are for calculations with surface-to-surface potential including the curvature correction.

In Fig. 6(a) one sees the dramatic effect of accounting for the curvature correction: whereas $\sigma_s(1)$ is above $\sigma_{\Delta r}(1)$, accounting for the curvature correction brings the cross sections $\sigma_s(G)$ substantially below $\sigma_{\Delta r}(1)$ at low energies. We have to conclude that at these energies, for positive values of β_4, the impact of the curvature correction on the fusion cross sections appears to be significantly stronger than the effect of the minimum distance. The barrier distribution as a whole is affected more strongly by the minimum distance effect, as seen in Fig. 6(b).

Remarkably, the change of the sign of β_4 reduces the influence of both minimum distance and curvature on the absolute value of σ: in Fig. 6(c) the three curves are hardly distinguishable. However, in Fig. 6(d) the barrier distributions make it clear that the energy dependence of σ is affected by the minimum distance and curvature correction more strongly than for positive values of β_4. For both positive and negative β_4, the use of the surface-to-surface potential shifts the barrier distribution to lower energies, although this shift is compensated for to a certain extent by the curvature correction, especially for $\beta_4 < 0$.

In Fig. 7 the results of calculations of the fusion cross sections and barrier distributions for $^{16}O + ^{154}Sm$ are presented along with the data from Ref. [20]. These calculations are performed with $\beta_2 = 0.306$ and $\beta_4 = 0.13$. In Fig. 7(a) the fusion cross sections obtained with the surface-to-surface potential including the curvature correction (thick solid line) are compared with those for the center-line potential without the curvature correction (thin solid line). The dotted line represents the cross section calculated for a spherical target. Since fusion occurs mostly near the tip of the target for the

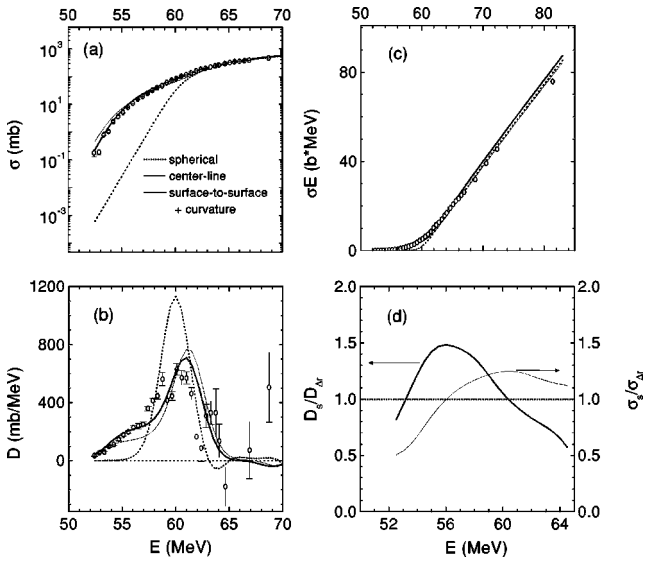

FIG. 7. Comparison of the fusion cross sections and barrier distributions (calculated for $\beta_2=0.306$, and $\beta_4=0.13$) with experimental data for the reaction $^{16}O+^{154}Sm$. Shown as a function of energy in the center-of-mass frame are (a) the fusion cross section σ, (b) the barrier distribution D, (c) the product σE, and (d) the ratios $D_s(G)/D_{\Delta r}(1)$ (thick solid line) and $\sigma_s(G)/\sigma_{\Delta r}(1)$ (thin solid line). In panels (a)–(c), dotted lines denote calculations for a spherical target, thin solid lines denote calculations with the center-line potential without curvature correction, and thick solid lines denote calculations with the surface-to-surface potential including the curvature correction. Open circles with error bars show the experimental data of Ref. [20].

low energies, $\sigma_s(G)$ are lower than $\sigma_{\Delta r}(1)$ due to the curvature correction. For the near-barrier energies the calculated fusion cross sections agree satisfactorily with the experimental data when deformation is accounted for. Results obtained with the surface-to-surface potential agree better with the data, though this depends upon the values of β_2 and β_4 used.

The calculated barrier distributions are compared with each other and with the data in Fig. 7(b). As expected, the barrier distribution obtained with the spherical target (dotted line) is very sharply peaked and does not agree with the data even qualitatively. The main effect of the calculations with the surface-to-surface potential including the curvature correction is that the $D_s(G)$ (thick solid line) is shifted with respect to $D_{\Delta r}(1)$ (thin solid line) in the direction of lower fusion barriers—the effect already observed in Fig. 6(b). The calculated barrier distribution appears to be closer to the experimental one when the surface-to-surface potential is used.

In order to see the degree of agreement between calculated and measured cross sections at energies well above the barrier, in Fig. 7(c) we plot the excitation function of the product σE on a linear scale. At higher energies the results of the calculations are in a reasonable agreement with the data, although slightly above the experimental points no matter what potential is used. In order to show quantitatively the importance of changing from the center-line potential to the surface-to-surface potential, in Fig. 7(d) we plot the ratios of the cross sections $\sigma_s(G)/\sigma_{\Delta r}(1)$ (thin solid curve) and of the barrier distributions $D_s(G)/D_{\Delta r}(1)$ (thick solid curve) as a function of energy. These ratios vary by up to 50%, indicating the importance of accounting for both the minimum distance and the curvature correction in calculating the nuclear potential.

VI. CONCLUSION

Our starting point was that the Woods-Saxon center-line nucleus-nucleus potential ignoring the surface curvature correction may not be adequate in the calculation of the fusion cross sections performed by means of the simplified coupled channels codes like CCDEF [5] and CCMOD [6]. We have shown that using the minimum distance between the surfaces of the fusing nuclei as the argument of the nuclear potential and accounting for the curvature correction substantially affects the calculated fusion cross sections σ and barrier distributions D, if the target nucleus has a large static deformation. These quantities can change by up to 50% for the $^{16}O+^{154}Sm$ reaction. Since current experimental data have typical precisions of 1% for σ and of 10% for D (see Refs. [3,7,20]), accounting for these geometrical effects is necessary in data analysis and interpretation. Our conclusions do not depend sensitively upon the type of internucleus potential; therefore, they are expected to also hold for more rigorous coupled channels codes like ECIS [26], FRESCO [27], and CCFULL [28], which use the Woods-Saxon center-line potential.

ACKNOWLEDGMENTS

M.D. acknowledges the financial support of the Australian Research Council.

[1] R.G. Stokstad, Y. Eisen, S. Kaplanis, D. Pelte, U. Smilansky, and I. Tserruya, Phys. Rev. Lett. **41**, 465 (1978).
[2] N. Rowley, G.R. Satchler, and P.H. Stelson, Phys. Lett. B **254**, 25 (1991).
[3] J.R. Leigh, N. Rowley, R.C. Lemmon, D.J. Hinde, J.O. Newton, J.X. Wei, J.C. Mein, C.R. Morton, S. Kuyucak, and A.T. Kruppa, Phys. Rev. C **47**, R437 (1993).
[4] A.M. Stefanini, D. Ackermann, L. Corradi, D.R. Napoli, C. Petrache, P. Spolaore, P. Bednarczyk, H.Q. Zhang, S. Beghini, G. Montagnoli, L. Mueller, F. Scarlassara, G.F. Segato, F. Soramel, and N. Rowley, Phys. Rev. Lett. **74**, 864 (1995).
[5] C.H. Dasso and S. Landowne, Comput. Phys. Commun. **46**, 187 (1987); J.O. Fernández Niello, C.H. Dasso, and S. Landowne, *ibid.* **54**, 409 (1989).
[6] M. Dasgupta, A. Navin, Y.K. Agarwal, C.V.K. Baba, H.C. Jain, M.L. Jhingan, and A. Roy, Nucl. Phys. **A539**, 351 (1992).
[7] M. Dasgupta, D.J. Hinde, N. Rowley, and A.M. Stefanini, Annu. Rev. Nucl. Part. Sci. **48**, 401 (1998).
[8] R. W. Hasse and W. D. Myers, *Geometrical Relationships of Macroscopic Nuclear Physics* (Springer-Verlag, Berlin, 1988), p. 47.
[9] J. Randrup and J.S. Vaagen, Phys. Lett. **77B**, 170 (1978).

[10] A.J. Baltz and B.F. Bayman, Phys. Rev. C **26**, 1969 (1982); B.F. Bayman, *ibid.* **34**, 1346 (1986).
[11] D.L. Hendrie, Phys. Rev. Lett. **7**, 478 (1973).
[12] J. Blocki, J. Randrup, W.J. Swiatecki, and C.F. Tsang, Ann. Phys. (N.Y.) **105**, 437 (1977).
[13] M. Seiwert, W. Greiner, V. Oberacker, and M.J. Rhoades-Brown, Phys. Rev. C **29**, 477 (1984).
[14] N. Malhotra and R.K. Gupta, Phys. Rev. C **31**, 1179 (1985).
[15] R. A. Broglia, C. H. Dasso, and A. Winter, in *Proceedings of the International School of Physics "Enrico Fermi,"* Varenna Course, 1979, edited by R. A. Broglio, R. A. Ricci, and H. A. Dasso (North-Holland, Amsterdam, 1981), p. 327.
[16] P. Fröbrich, Phys. Rep. **116**, 337 (1984).
[17] J. Marten and P. Fröbrich, Nucl. Phys. **A545**, 854 (1992).
[18] D.H.E. Gross and H. Kalinowski, Phys. Rep. **45**, 175 (1978).
[19] P. Fröbrich (private communication).
[20] J.R. Leigh, M. Dasgupta, D.J. Hinde, J.C. Mein, C.R. Morton, R.C. Lemmon, J.P. Lestone, J.O. Newton, H. Timmers, J.X. Wei, and N. Rowley, Phys. Rev. C **52**, 3151 (1995).
[21] S. Raman, C.H. Malarkey, W.T. Milner, C.W. Nestor, Jr., and P.H. Stelson, At. Data **36**, 1 (1987).
[22] R.M. Stephens, R.M. Diamond, and J. de Boer, Phys. Rev. Lett. **27**, 1151 (1971).
[23] P. Möller, J.R. Nix, W.D. Myers, and W.J. Swiatecki, At. Data **59**, 185 (1995).
[24] G. A. Korn and T. M. Korn, *Mathematical Handbook for Scientists and Engineers* (McGraw-Hill, New York, 1968), p. 569.
[25] C.R. Morton, A.C. Berriman, R.D. Butt, M. Dasgupta, D.J. Hinde, A. Godley, J.O. Newton, and K. Hagino, Phys. Rev. C **64**, 034604 (2001).
[26] J. Raynal, Phys. Rev. C **23**, 2571 (1981).
[27] I.J. Thompson, Comput. Phys. Rep. **7**, 167 (1988).
[28] K. Hagino, N. Rowley, and A.T. Kruppa, Comput. Phys. Commun. **123**, 143 (1999).